AIAA SciTech Forum
6-10 January 2020, Orlando, FL
AIAA Scitech 2020 Forum

10.2514/6.2020-0109

Boundary layer receptivity analysis via the algebraic Lyapunov equation

Wei Ran *
University of Southern California, Los Angeles, CA, 90089, USA

Armin Zare †
University of Texas at Dallas, Richardson, TX, 75080, USA

M. J. Philipp Hack ‡
Stanford University, Stanford, CA, 94305

Mihailo R. Jovanović §
University of Southern California, Los Angeles, CA, 90089, USA

We use the algebraic Lyapunov equation to study the receptivity of pre-transitional boundary layers to persistent sources of stochastic excitation. The effect of exogenous disturbances is modeled using an additive stochastic forcing that enters at various wall-normal locations and the fluctuation dynamics are studied via linearized models that arise from locally parallel and global perspectives. Even though locally parallel analysis does not account for the effect of the spatially evolving base flow, we demonstrate that it captures the essential mechanisms and the prevailing length-scales. On the other hand, global analysis, which accounts for the spatially evolving nature of the boundary layer flow, predicts the amplification of a cascade of streamwise scales throughout the streamwise domain. We show that the flow structures that are extracted from a modal decomposition of the resulting velocity covariance matrix, can be closely captured by conducting locally parallel analysis at various streamwise locations and over different wall-parallel wavenumber pairs. Our approach does not rely on costly stochastic simulations and it provides insight into mechanisms for perturbation growth, including the interaction of the slowly varying base flow with streaks and Tollmien-Schlichting waves.

I. Introduction

Laminar-turbulent transition of fluid flows is important in many engineering applications. In the laminar boundary layer flow, disturbances are amplified either through modal, i.e., exponential, instability mechanisms or non-modal amplification, e.g., via transient growth mechanisms such as lift-up [1, 2] and Orr mechanisms [3–5]. An important aspect in both scenarios is the receptivity of the boundary layer flow to external excitation sources, e.g., free-stream turbulence and surface roughness. Such sources of excitation perturb the velocity field and give rise to initial disturbances within the shear that can grow to critical levels. The effect of free-stream turbulence on the growth of streaks has been the subject of various experimental [6–8], numerical [9, 10], and theoretical [11, 12] studies. In particular, it has been shown that free-stream disturbances that penetrate into the boundary layer are elongated in the streamwise direction [13]. While nonlinear models that are based on the Navier-Stokes (NS) equations provide insight into receptivity mechanisms, their implementation typically involves a large number of degrees of freedom. This motivates the development of low-complexity models that are better suited for comprehensive quantitative studies.

While the nonlinear terms in the NS equations play an important role in transition to turbulence and in sustaining the turbulent state, they are conservative and, as such, they do not contribute to the transfer of energy between the mean flow and velocity fluctuations but only transfer energy between different Fourier modes [14, 15]. This feature has inspired modeling the effect of nonlinearity using additive stochastic forcing with early efforts focused on homogeneous isotropic turbulence [16–18]. In the presence of stochastic excitation, the linearized NS equations have been used to

*Graduate student, Aerospace and Mechanical Engineering, AIAA Student Member
†Assistant Professor, Mechanical Engineering, IEEE Member, AIAA Member
‡Research Associate, Center for Turbulence Research, AIAA member
§Professor, Electrical and Computer Engineering, IEEE Fellow

characterize the most detrimental stochastic forcing and determine scaling laws for energy amplification at subcritical Reynolds numbers [19–21], and to replicate structural [22, 23] and statistical [24, 25] features of wall-bounded turbulent flows. In these studies, stochastic forcing has been commonly used to model the impact of exogenous excitation sources and initial conditions, or to capture the effect of nonlinearity in the NS equations.

While in parallel flows, homogeneity in the wall-parallel dimensions allows for the decoupling of the governing equations via application of the Fourier transform, in the flat-plate boundary layer, streamwise and wall-normal inhomogeneity require discretization over two spatial directions and lead to models of significantly larger sizes. Conducting modal and non-modal analyses is thus more challenging than for locally parallel flows. However, due to the slowly varying nature of the boundary layer flow, parallel flow assumptions can still provide meaningful results. For example, primary disturbances can be identified using the eigenvalue analysis of the Orr-Sommerfeld and Squire equations [26] and the secondary instabilities can be obtained via Floquet analysis [27]. Moreover, the NS equations can be parabolized to account for the downstream propagating nature of waves in slowly varying flows via spatial marching. This technique has enabled the analysis of transitional boundary layers and turbulent jet flows using various forms of the unsteady boundary-region equations [28, 29], parabolized stability equations [30, 31], one-way Euler equations [32], and the more recent parabolized Floquet equations [33].

The parallel flow assumption offers significant computational advantages, but it does not account for the effect of the spatially evolving base flow on the stability of the boundary layer. Global stability analysis addresses this issue by accounting for the spatially varying nature of the base flow and discretizing all inhomogeneous dimensions. Previously, tools from sparse linear algebra in conjunction with iterative schemes have been employed to analyze the eigenspectrum of the governing equations and provide insight into the dynamics of transitional flows [34–38]. Efforts have also been made to conduct non-modal analysis of spatially evolving flows including transient growth [39, 40] and resolvent [41–44] analyses. However, previous studies did not incorporate information regarding the spatio-temporal spectrum and spatial localization of excitation sources. Moreover, the widely used resolvent analysis [45–47] is limited to monochromatic forcing and, as such, may not fully capture naturally occurring sources of excitation.

The approach advanced in the present work enables the study of receptivity mechanisms in boundary layer flows subject to stochastic sources of excitation. We model the effect of free-stream turbulence as a persistent white-in-time stochastic forcing that enters at various wall-normal locations and analyze the dynamics of velocity fluctuations around locally parallel and spatially evolving base flows using the solution to the algebraic Lyapunov equation. Our simulation-free approach enables computationally efficient assessment of the energy spectrum of spatially evolving flows, without relying on a particular form of the inflow conditions or computation of the full spectrum of the linearized dynamical generator. Moreover, the broad-band nature of our forcing model captures the aggregate effect of all time-scales without the need to integrate the frequency response over all energetically relevant frequencies. Our results demonstrate that global covariance matrices cannot be well-approximated by low-rank representations. On the other hand, locally parallel analysis, which breaks up the receptivity process of the boundary layer flow over various streamwise length-scales, can uncover certain flow structures that are difficult to observe in global analysis.

The paper is organized as follows. In Section II, we introduce the stochastically forced linearized NS equations and describe the algebraic Lyapunov equation that we use to compute second-order statistics of velocity fluctuations, extract information about the energy amplification, and identify energetically dominant flow structures. In Section III, we study the receptivity to stochastic excitations of the velocity fluctuations around a locally parallel Blasius boundary layer profile. In Section IV, we extend the receptivity analysis to stochastically forced non-parallel flows and compare the results of locally parallel and global analyses. We provide concluding remarks in Section V.

II. Stochastically forced linearized NS equations

In a flat-plate boundary layer, the linearized incompressible NS equations around the Blasius base flow profile $\bar{\mathbf{u}} = [\, U(x,y) \;\; V(x,y) \;\; 0 \,]^T$ are given by

$$\begin{aligned} \mathbf{v}_t &= -(\nabla\cdot\bar{\mathbf{u}})\,\mathbf{v} \;-\; (\nabla\cdot\mathbf{v})\,\bar{\mathbf{u}} \;-\; \nabla p \;+\; \frac{1}{Re_0}\,\Delta\mathbf{v} \;+\; \mathbf{d}, \\ 0 &= \nabla\cdot\mathbf{v}, \end{aligned} \tag{1}$$

where $\mathbf{v} = [\, u \;\; v \;\; w \,]^T$ is the vector of velocity fluctuations, p denotes pressure fluctuations, u, v, and w represent components of the fluctuating velocity field in the streamwise (x), wall-normal (y), and spanwise (z) directions, and $\mathbf{d}$ denotes an additive zero-mean stochastic body forcing. The stochastic perturbation $\mathbf{d}$ is used to model the effect of exogenous sources of excitation on the boundary layer flow and, as illustrated in Fig. 1, it can be introduced in various wall-normal regions. In Eqs. (1), $Re_0 = U_\infty \delta_0/\nu$ is the Reynolds number based on the Blasius length-scale

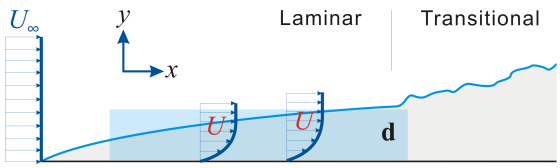

Fig. 1 Geometry of boundary layer flow with stochastic excitation d entering in the blue shaded region.

$\delta_0 = \sqrt{\nu\, x_0/U_\infty}$, where the initial streamwise location x_0 denotes the distance from the leading edge, U_∞ is the free-stream velocity, and ν is the kinematic viscosity. The local Reynolds number at distance x to the starting position x_0 is thus given by $Re = Re_0\sqrt{1 + x/x_0}$. The velocities are non-dimensionalized by U_∞, time by δ_0/U_∞, and pressure by ρU_∞^2, where ρ is the fluid density.

A. Evolution model

Elimination of the pressure yields an evolution form of the linearized equations with the state variable $\boldsymbol{\varphi} = [\, v \;\; \eta \,]^T$, which contains the wall-normal velocity v and vorticity $\eta = \partial_z u - \partial_x w$ [26]. In addition, homogeneity of the Blasius base flow in the spanwise direction allows a normal-mode representation with respect to z, yielding the evolution model

$$\begin{aligned} \partial_t \boldsymbol{\varphi}(x, y, k_z, t) &= [\mathbf{A}(k_z)\, \boldsymbol{\varphi}(\cdot, k_z, t)](x, y) \;+\; [\mathbf{B}(k_z)\, \mathbf{d}(\cdot, k_z, t)](x, y), \\ \mathbf{v}(x, y, k_z, t) &= [\mathbf{C}(k_z)\, \boldsymbol{\varphi}(\cdot, k_z, t)](x, y), \end{aligned} \tag{2}$$

which is parameterized by the spanwise wavenumber k_z. Definitions of the operators $\mathbf{A}$, $\mathbf{B}$, and $\mathbf{C}$ are provided in [48, Appendix A]. We note that an additional wall-parallel base flow assumption that entails $\bar{\mathbf{u}} = [\, U(y) \;\; 0 \;\; 0 \,]^T$ renders the coefficients in Eqs. (1) independent of x and thus enables a normal-mode representation in that dimension as well.

We obtain finite-dimensional approximations of the operators in Eqs. (2) using a pseudospectral discretization scheme [49] in the spatially inhomogeneous directions. For streamwise-varying base flows we consider N_x and N_y Chebyshev collocation points in x and y, and for streamwise invariant base flows we use N_y points in y. Furthermore, a change of variables is employed to obtain a state-space representation in which the kinetic energy is determined by the Euclidean norm of the state vector; see [48, Appendix B]. We thus arrive at the state-space model

$$\begin{aligned} \dot{\boldsymbol{\psi}}(t) &= A\, \boldsymbol{\psi}(t) \;+\; B\, \mathbf{d}(t), \\ \mathbf{v}(t) &= C\, \boldsymbol{\psi}(t), \end{aligned} \tag{3}$$

where $\boldsymbol{\psi}(t)$ and $\mathbf{v}(t)$ are vectors with $2N_xN_y$ and $3N_xN_y$ complex-valued components, respectively ($2N_y$ and $3N_y$ components, respectively, for parallel flows), and state-space matrices A, B, and C incorporate the aforementioned change of variables and wavenumber parameterization over k_z (over (k_x, k_z) for parallel flows).

B. Second-order statistics of velocity fluctuations

We next characterize the structural dependence between the second-order statistics of the state and forcing term in the linearized dynamics. We also describe how the energy amplification arising from persistent stochastic excitation and the energetically dominant flow structures can be computed from these flow statistics. All mathematical statements in the remainder of this section are parameterized over homogeneous directions.

In statistical steady-state, the covariance matrices $\Phi = \lim_{t\to\infty} \langle \mathbf{v}(t)\, \mathbf{v}^*(t) \rangle$ of the velocity fluctuation vector and $X = \lim_{t\to\infty} \langle \boldsymbol{\psi}(t)\, \boldsymbol{\psi}^*(t) \rangle$ of the state vector in Eq. (3) are related by

$$\Phi \;=\; C\, X\, C^*, \tag{4}$$

where $\langle \cdot \rangle$ denotes the expectation and superscript $*$ denotes complex conjugate transpose. The matrix Φ contains information about all second-order statistics of the fluctuating velocity field in statistical steady-state, including the Reynolds stresses. We assume that the persistent source of excitation $\mathbf{d}(t)$ in Eq. (3) is zero-mean and white-in-time with spatial covariance matrix $W = W^*$,

$$\langle \mathbf{d}(t_1)\, \mathbf{d}^*(t_2) \rangle \;=\; W\, \delta(t_1 - t_2), \tag{5}$$

where δ is the Dirac delta function. When the linearized dynamics (3) are stable, the steady-state covariance X of the state $\boldsymbol{\psi}(t)$ can be determined as the solution to the algebraic Lyapunov equation

$$A\,X \;+\; X\,A^{*} \;=\; -B\,W\,B^{*}. \tag{6}$$

The Lyapunov equation (6) relates the statistics of white-in-time forcing, represented by W, to the infinite-horizon state covariance X via system matrices A and B. It can also be used to compute the energy spectrum of velocity fluctuations $\mathbf{v}$,

$$E \;=\; \mathrm{trace}\,(\Phi) \;=\; \mathrm{trace}\,\left(C\,X\,C^{*}\right). \tag{7}$$

We note that the steady-state velocity covariance matrix Φ can be alternatively obtained from the spectral density matrix of velocity fluctuations $S_{\mathbf{v}}(\omega)$ as [50],

$$\Phi \;=\; \frac{1}{2\pi}\int_{-\infty}^{\infty} S_{\mathbf{v}}(\omega)\,\mathrm{d}\omega.$$

For the linearized NS equations $S_{\mathbf{v}}(\omega) := T_{\mathbf{vd}}(\omega)\,W\,T_{\mathbf{vd}}^{*}(\omega)$, where the frequency response matrix

$$T_{\mathbf{vd}}(\omega) \;=\; C\,(\mathrm{i}\omega I \;-\; A)^{-1}\,B,$$

is obtained by applying the temporal Fourier transform on system (3). We note that the solution X to the algebraic Lyapunov equation (6) allows us to avoid integration over temporal frequencies and compute the energy spectrum E using (7); see [48, Section V.B] for additional details.

Following the proper orthogonal decomposition of [51, 52], the velocity field can be decomposed into characteristic eddies by determining the spatial structure of fluctuations that contribute most to the energy amplification. For turbulent channel flow, it has been shown that the dominant characteristic eddy structures extracted from second-order statistics of the stochastically forced linearized model qualitatively agree with results obtained using eigenvalue decomposition of DNS-generated autocorrelation matrices; see Figs. 15 in [24] and [52]. In addition to examining the energy spectrum of velocity fluctuations, we will use the eigenvectors of the covariance matrix Φ (defined in Eq. (4)) to study dominant flow structures that are triggered by stochastic excitation.

Remark 1 *Since linearized dynamics* (3) *are globally stable even when the flow is convectively unstable [53], the Lyapunov-based approach can be used to conduct the steady-state analysis of the velocity fluctuations statistics for many flow configurations that are not stable from the perspective of local analysis.*

C. Filtered excitation and receptivity coefficient

Let us specify the spatial region in which the forcing enters, by introducing $\mathbf{d}(x, y, z, t) := f(y)\,h(x)\,\mathbf{d}_s(x, y, z, t)$, where $\mathbf{d}_s$ represents a white solenoidal forcing, $f(y)$ is a smooth filter function defined as

$$f(y) \;:=\; \frac{1}{\pi}\left(\mathrm{atan}\left(a\,(y \;-\; y_1)\right) \;-\; \mathrm{atan}\left(a\,(y \;-\; y_2)\right)\right), \tag{8}$$

and $h(x)$ is a filter function that determines the streamwise extent of the forcing. Here, y_1 and y_2 determine the wall-normal extent of $f(y)$ and a specifies the roll-off rate; Fig. 2 shows $f(y)$ with $y_1 = 5$ and $y_2 = 10$, for two cases of $a = 1$ and $a = 10$. In Sections III and IV, we study energy amplification arising from stochastic excitation that enters at various wall-normal locations; see Table 1. For the near-wall forcing (with $y_1 = 0$ and $y_2 = 5$) with $a = 1$, more than 96% of the energy of the forcing is applied within the $\delta_{0.99}$ boundary layer thickness; on the other hand, for the outer-layer forcing (with $y_1 = 15$ and $y_2 = 20$) with $a = 1$, less than 0.1% is applied in that region.

We quantify the receptivity of velocity fluctuations to stochastic forcing that enters at various wall-normal regions using the receptivity coefficient

$$C_R \;:=\; \frac{\lim_{t\to\infty}\left\langle (D_g\mathbf{v}(t))^{*} D_g\mathbf{v}(t)\right\rangle}{\lim_{t\to\infty}\langle \mathbf{d}^{*}(t)\,\mathbf{d}(t)\rangle} \;=\; \frac{\mathrm{trace}\left(D_g\Phi D_g^{*}\right)}{\mathrm{trace}\,(W)}, \tag{9}$$

which determines the ratio of the energy of velocity fluctuations within the boundary layer to the energy of the forcing. Here, $D_g := g(x, y)I$, where the function $g(x, y)$ is a top-hat filter that extracts velocity fluctuations within the $\delta_{0.99}$ boundary layer thickness. In parallel flows, the function g is invariant with respect to the streamwise direction.

Table 1 Cases of stochastic excitation entering at various wall-normal regions

case number	wall-normal region of excitation; $[\, y_1,\ y_2\,]$ in Eq. (8)
1 (near-wall)	[0, 5]
2	[5, 10]
3	[10, 15]
4 (outer-layer)	[15, 20]

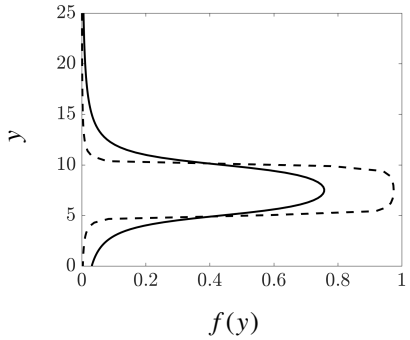

Fig. 2 The shape of the filter function $f(y)$ for $y_1 = 5$, $y_2 = 10$ with $a = 1$ (−) and $a = 10$ (−−).

III. Receptivity analysis of locally parallel flow

We first examine the dynamics of the stochastically forced Blasius boundary layer under the locally parallel flow assumption. In this case, the base flow only depends on the wall-normal coordinate y and evolution model (3) is parameterized by horizontal wavenumbers (k_x, k_z), which significantly reduces the computational complexity. We perform an input-output analysis to quantify the energy amplification of velocity fluctuations subject to free-stream turbulence.

We compute the energy spectrum of stochastically excited parallel Blasius boundary layer flow with $Re_0 = 232$ (the Blasius length-scale is $\delta_0 = 1$). Here, we consider a wall-normal region with $L_y = 35$ and discretize the differential operators in Eqs. (2) using $N_y = 100$ Chebyshev collocation points in y. In the wall-normal direction, homogenous Dirichlet boundary conditions are imposed on wall-normal vorticity, $\eta(0) = \eta(L_y) = 0$ and Dirichlet/Neumann boundary conditions are imposed on wall-normal velocity, $v(0) = v(L_y) = 0$, $v_y(0) = v_y(L_y) = 0$, where v_y denotes the derivative of v with respect to y. In the horizontal directions, we use 50×51 logarithmically spaced wavenumbers with $k_x \in [10^{-4}, 1]$ and $k_z \in [5 \times 10^{-3}, 10]$ to parameterize the linearized model (3). Thus, for each pair (k_x, k_z), the state $\boldsymbol{\psi} = [\, v^T \ \ \eta^T \,]^T$ is a complex-valued vector with $2N_y$ components. Grid convergence has been verified by doubling the number of points used in the discretization of the differential operators in the wall-normal coordinate.

We first consider a streamwise invariant ($h(x) = 1$) solenoidal white-in-time excitation $\mathbf{d}$ with covariance $W = I$ in the immediate vicinity of the wall (case 1 in Table 1). Figure 3(a) shows largest receptivity at low streamwise wavenumbers ($k_x \approx 0$) with a global peak at $k_z \approx 0.25$. This indicates that streamwise elongated streaks are the dominant flow structures that result from persistent stochastic excitation of the boundary layer flow. Such streamwise elongated structures are reminiscent of energetically dominant streaks with spanwise wavenumbers $k_z \approx 0.26$ (in Blasius length-scale) that were identified in analyses of optimal disturbances [54, 55]. Slightly smaller spanwise wavenumbers have been recorded from hot-wire signal correlations in the boundary layer subject to free-stream turbulence [6]. In addition to streaks, Fig. 3(a) also predicts the emergence of TS waves at $k_x \approx 0.19$. For outer-layer forcing, the amplification of streamwise elongated structures persists while the amplification of the TS waves weakens; see Fig. 3(b). It is also observed that as the region of excitation moves away from the wall, energy amplification becomes weaker and the peak of the receptivity coefficient shifts to lower values of k_z. As we demonstrate in Section IV, these observations are in agreement with the global receptivity analysis of stochastically excited boundary layer flow.

The one-dimensional energy spectrum shown in Fig. 4(a) quantifies the energy amplification E over various spanwise wavenumbers when forcing enters at different distances from the wall. This quantity can be computed by integrating the

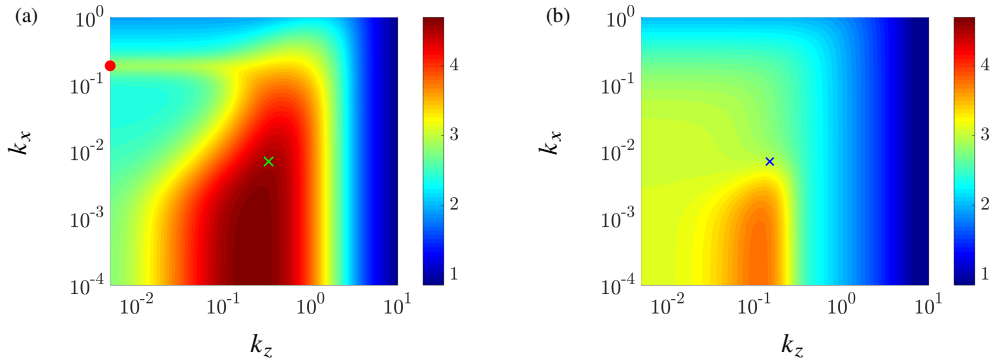

Fig. 3 Plots of $\log_{10}(C_R(k_x, k_z))$ in the parallel Blasius boundary layer flow with $Re_0 = 232$ subject to (a) near-wall, and (b) outer-layer white-in-time stochastic excitation. The dot and crosses respectively mark the wavenumber pairs associated with TS waves and streaks that are closely examined in this paper.

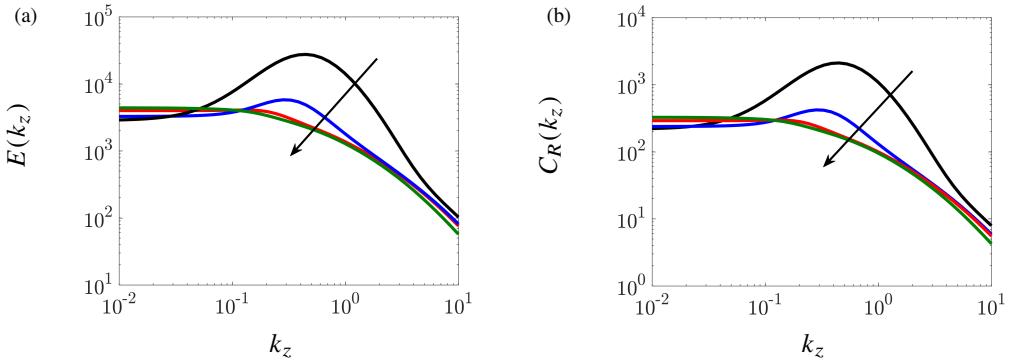

Fig. 4 (a) The one-dimensional energy spectrum, and (b) the receptivity coefficient for the parallel Blasius boundary layer flow with $Re_0 = 232$ subject to white stochastic excitation entering in the wall-normal regions covered in Table 1; case 1 (black), case 2 (blue), case 3 (red), and case 4 (green). The forcing region moves away from the wall in the direction of the arrows.

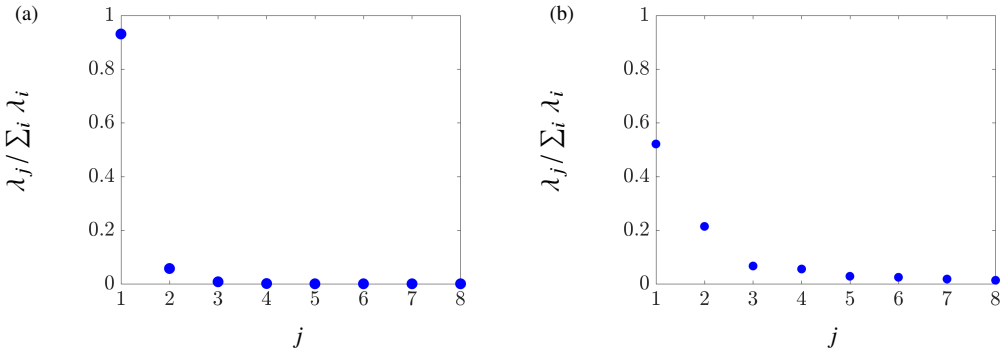

Fig. 5 Contribution of the first 8 eigenvalues of the velocity covariance matrix Φ of the Blasius boundary layer flow with $Re_0 = 232$ subject to (a) near-wall, and (b) outer-layer white-in-time stochastic forcing.

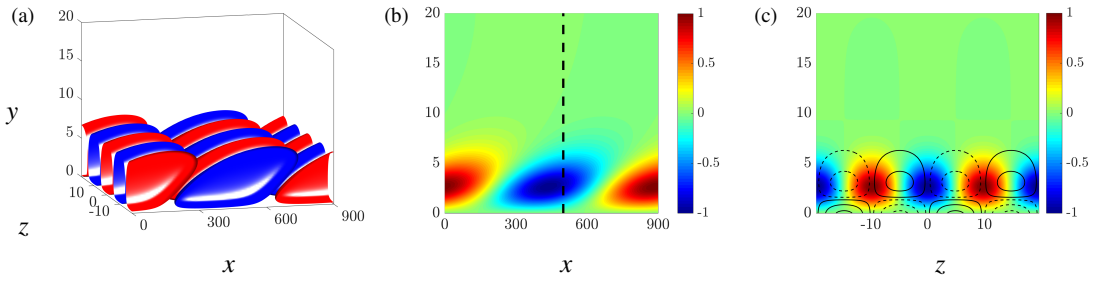

Fig. 6 Principal modes with $(k_x, k_z) = (7 \times 10^{-3}, 0.32)$, resulting from excitation of the boundary layer flow with $Re_0 = 232$ in the vicinity of the wall. (a) Streamwise velocity component where red and blue colors denote regions of high and low velocity. (b) Streamwise velocity at $z = 0$. (c) y-z slice of streamwise velocity (color plots) and vorticity (contour lines) at $x = 500$, which corresponds to the cross-plane slice indicated by the black dashed lines in (b).

energy spectrum $E(k_x, k_z)$ (cf. Eq. (7)) over streamwise wavenumbers. In Fig. 4, the locations at which the energy spectrum peaks correspond to the spanwise scale associated with streamwise elongated streaks. When the forcing region shifts away from the wall, the energy amplification decreases, indicating that the flow region in the immediate vicinity of the wall is more susceptible to external excitation. As mentioned earlier, we also observe that, when the forcing region shifts upward, the boundary layer streaks become wider in the spanwise direction. Figure 4(b) shows similar trends in the receptivity coefficient as a function of spanwise wavenumber k_z, which is computed by integrating C_R presented in Fig. 3 over streamwise wavenumbers.

While the sum of all eigenvalues of the matrix Φ determines the overall energy amplification reported in Fig. 4(a), it is also useful to examine the spatial structure of modes with dominant contribution to the energy of the flow. Figure 5 shows the contribution of the first 8 eigenvalues of Φ to the energy amplification, $\lambda_j / \sum_i \lambda_i$ when the boundary layer flow is subject to stochastic forcing. For fluctuations with $(k_x, k_z) = (7 \times 10^{-3}, 0.32)$ and near-wall excitation (cross in Fig. 3(a)) the principal mode which corresponds to the largest eigenvalue, contains approximately 93% of the total energy. On the other hand, for fluctuations with $(k_x, k_z) = (7 \times 10^{-3}, 0.15)$ and outer-layer excitation (cross in Fig. 3(b)) the principal mode contains approximately 52% of the total energy. The eigenvalue decomposition of the velocity covariance matrix Φ can be used to identify the energetically dominant flow structures resulting from stochastic excitation. Figures 6 and 7 show the flow structures associated with the streamwise component of these most significant modes. From Figs. 6(b) and 7(b) it is evident that the core of streamwise elongated structures moves away from the wall with the shift of the stochastically excited region. These streamwise elongated structures are situated between counter-rotating vortical motions in the cross-stream plane (cf. Figs. 6(c) and 7(c)) and contain alternating regions of fast- and slow-moving fluid, which are slightly inclined (and detached) relative to the wall. Even though these structures do not capture the full complexity of transitional flow, as we show in Section IV, they contain information

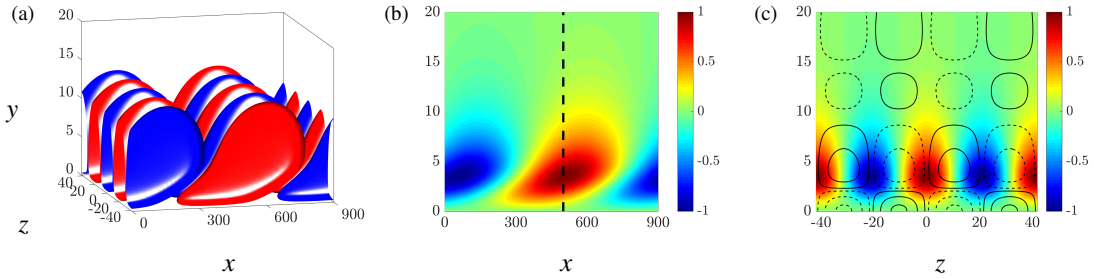

Fig. 7 Principal modes with $(k_x, k_z) = (7 \times 10^{-3}, 0.15)$, resulting from outer-layer excitation of the boundary layer flow with $Re_0 = 232$. (a) Streamwise velocity component where red and blue colors denote regions of high and low velocity. (b) Streamwise velocity at $z = 0$. (c) y-z slice of streamwise velocity (color plots) and vorticity (contour lines) at $x = 500$, which corresponds to the cross-plane slice indicated by the black dashed lines in (b).

about energetic streamwise elongated flow structures that are amplified by external excitation of the boundary layer flow. In particular, such alignment of counter-rotating vortices and streaks is closely related to the lift-up mechanism and the generation of streamwise elongated streaks [54–56].

IV. Global analysis of stochastically forced linearized NS equations

The parallel flow assumption applied in Section III allows for the efficient parameterization of the governing equations over all wall-parallel wavenumbers k_x and k_z. While this significantly reduces computational complexity, it excludes the effect of the spatially evolving base flow on the dynamics of velocity fluctuations. In global stability analysis, the NS equations are linearized around a spatially evolving Blasius boundary layer profile and the finite dimensional approximation is obtained by discretizing all inhomogeneous spatial directions. In this section, we employ global receptivity analysis to quantify the influence of stochastic excitation on the velocity fluctuations around the spatially evolving Blasius boundary layer base flow. We also provide connections between the spatial flow structures obtained via locally parallel and global analyses.

At any spanwise wavenumber k_z, the state $\boldsymbol{\psi} = [\, v^T \;\; \eta^T \,]^T$ of linearized evolution model (3) is a complex vector with $2N_xN_y$ components, where N_x and N_y denote the number of collocation points used to discretize the differential operators in the streamwise and wall-normal directions, respectively. We consider a Reynolds number $Re_0 = 232$ and a computational domain with $L_x = 900$ and $L_y = 35$, where the differential operators are discretized using $N_x = 101$ and $N_y = 50$ Chebyshev collocation points in x and y, respectively. Similar to locally parallel analysis, we verify convergence by doubling the number of grid points. As in Section III, in the wall-normal direction we enforce homogenous Dirichlet boundary conditions on η and homogeneous Dirichlet/Neumann boundary conditions on v. At the inflow, we impose homogeneous Dirichlet boundary conditions on η, i.e., $\eta(0, y) = 0$, and homogeneous Dirichlet/Neumann boundary conditions on v, i.e., $v(0, y) = v_y(0, y) = 0$. At the outflow, we apply linear extrapolation conditions on both state variables (v, η) and the streamwise derivative of the wall-normal component (v_y); see [57] for details. We also introduce sponge layers at the inflow and outflow to mitigate the influence of boundary conditions on the fluctuation dynamics within the computational domain [58].

For boundary layer flows, the global operator in Eqs. (3) has no exponentially growing eigenmodes [53]; see Remark 1. Thus, the steady-state covariance of the fluctuating velocity field can be obtained from the solution to Lyapunov equation (6) and the energy amplification can be computed using Eq. (7). As in Section III, we examine the influence of streamwise-invariant white-in-time stochastic forcing with covariance $W = I$ which enters at various wall-normal regions; this is achieved by filtering the forcing using the function $f(y)$ in (8). Figure 8 shows the k_z-dependence of energy amplification and receptivity coefficient for stochastic excitation entering at various wall-normal regions. Our computations show that the energy amplification increases as the region of influence for the external forcing approaches the wall, which qualitatively matches the result of the locally parallel analysis in Section III. In particular, for $Re_0 = 232$, the energy amplification reduces from 2.0×10^6 (for stochastic excitation that enters in the vicinity of the wall (case 1 in Table 1) with $k_z = 0.32$) to 9.6×10^4 (for stochastic excitation that enters away from the wall (case 4 in Table 1) with $k_z = 0.21$). Moreover, the structures that correspond to the largest energy amplification or receptivity coefficient become slightly wider in the spanwise direction, but this shift to smaller values of k_z is not as pronounced as in parallel flows (cf. Fig. 4). The largest energy amplification and receptivity are observed for structures with $k_z \in [0.21, 0.32]$,

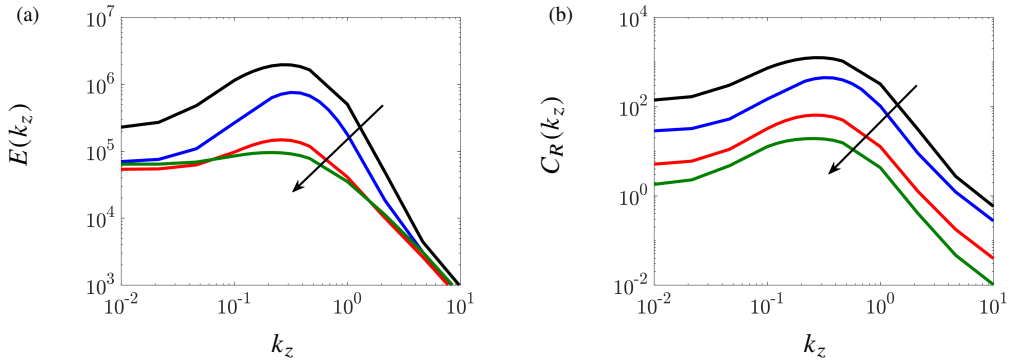

Fig. 8 (a) Energy amplification and (b) receptivity coefficient resulting from stochastic excitation of the linearized NS equations around a spatially varying Blasius profile with $Re_0 = 232$. Stochastic forcing enters at the wall-normal regions covered in Table 1; case 1 (black), case 2 (blue), case 3 (red), and case 4 (green). The forcing region moves away from the wall in the direction of the arrows.

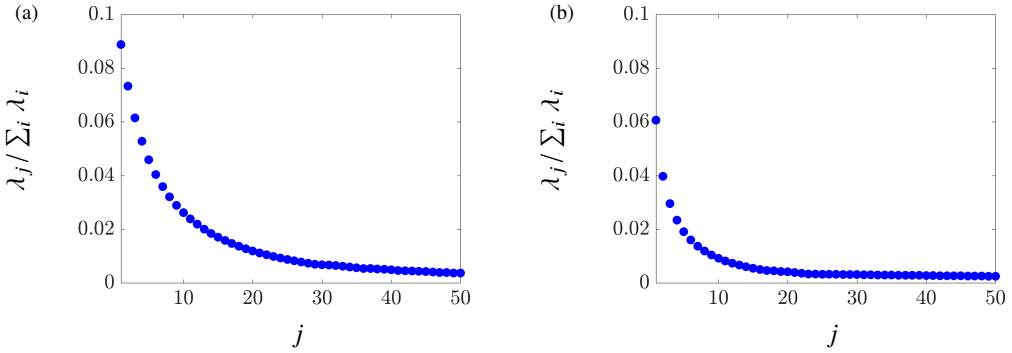

Fig. 9 Contribution of the first 50 eigenvalues of the velocity covariance matrix Φ of the Blasius boundary layer flow with $Re_0 = 232$ subject to white-in-time stochastic forcing (a) in the vicinity of the wall with spanwise wavenumber $k_z = 0.32$; and (b) away from the wall with spanwise wavenumber $k_z = 0.21$.

which is in close agreement with previous experimental [6] and theoretical studies [54, 55].

For $k_z = 0.32$, Fig. 9 shows the contribution of the first 50 eigenvalues of the velocity covariance matrix Φ resulting from near-wall and outer-layer stochastic excitation. In contrast to locally parallel analysis (cf. Fig. 5), we observe that other eigenvalues play a more prominent role. The implication is that in global analysis the principal eigenmode of Φ cannot capture the full complexity of the spatially evolving flow. Nevertheless, we examine the shape of such flow structures to gain insight into the effect of stochastic excitation on the eigenmodes of the covariance matrix Φ that comprise the fluctuation field. Figures 10(a) and 11(a) show the spatial structure of the streamwise component of the principal response to white-in-time stochastic forcing that enters in the vicinity of the wall and in the outer-layer, respectively. The streamwise growth of the streaks can be observed. Figures 10(b) and 11(b) display the cross-section of these streamwise elongated structures at $z = 0$. As the forcing region gets detached from the wall, the cores of the streaky structures also move away from it. As shown in Figs. 10(c) and 11(c), these streaky structures are situated between counter-rotating vortical motions in the cross-stream plane and they contain alternating regions of fast- and slow-moving fluid that are slightly inclined to the wall.

We next examine the spatial structure of less energetic eigenmodes of Φ. As illustrated in Fig. 9(a), for near-wall stochastic forcing the first six eigenmodes respectively contribute 8.9%, 7.3%, 6.1%, 5.3%, 4.6%, and 4.0% to the total energy amplification. We again use the streamwise velocity component to study the spatial structure of the corresponding eigenmodes. As shown in Fig. 12(b), while the principal mode consists of a single streamwise-elongated streak, the second mode is comprised of two shorter high- and low-speed streaks. Similarly, the third and fourth modes

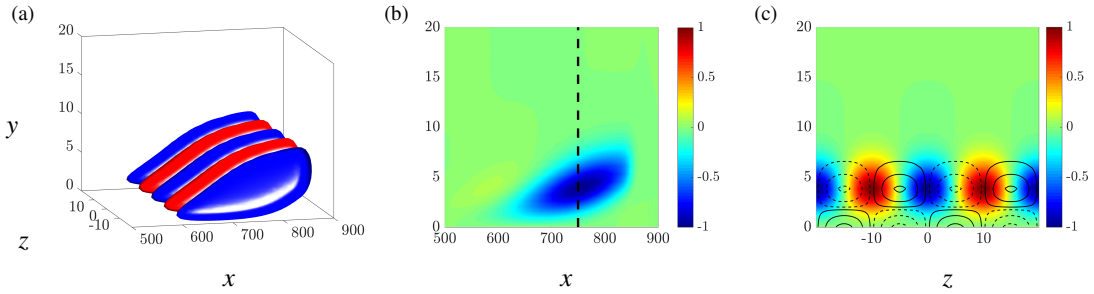

Fig. 10 Principal modes with $k_z = 0.32$, resulting from near-wall excitation of the boundary layer flow (case 1 in Table 1) with $Re_0 = 232$. (a) Streamwise velocity component where red and blue colors denote regions of high and low velocity. (b) Streamwise velocity at $z = 0$. (c) y-z slice of streamwise velocity (color plots) and vorticity (contour lines) at $x = 750$, which corresponds to the cross-plane slice indicated by the black dashed lines in (b).

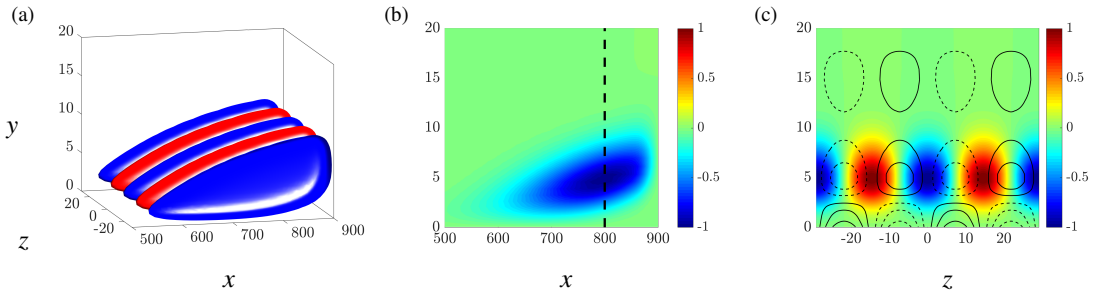

Fig. 11 Principal modes with $k_z = 0.21$, resulting from outer-layer excitation of the boundary layer flow (case 4 in Table 1) with $Re_0 = 232$. (a) Streamwise velocity component where red and blue colors denote regions of high and low velocity. (b) Streamwise velocity at $z = 0$. (c) y-z slice of streamwise velocity (color plots) and vorticity (contour lines) at $x = 800$, which corresponds to the cross-plane slice indicated by the black dashed lines in (b).

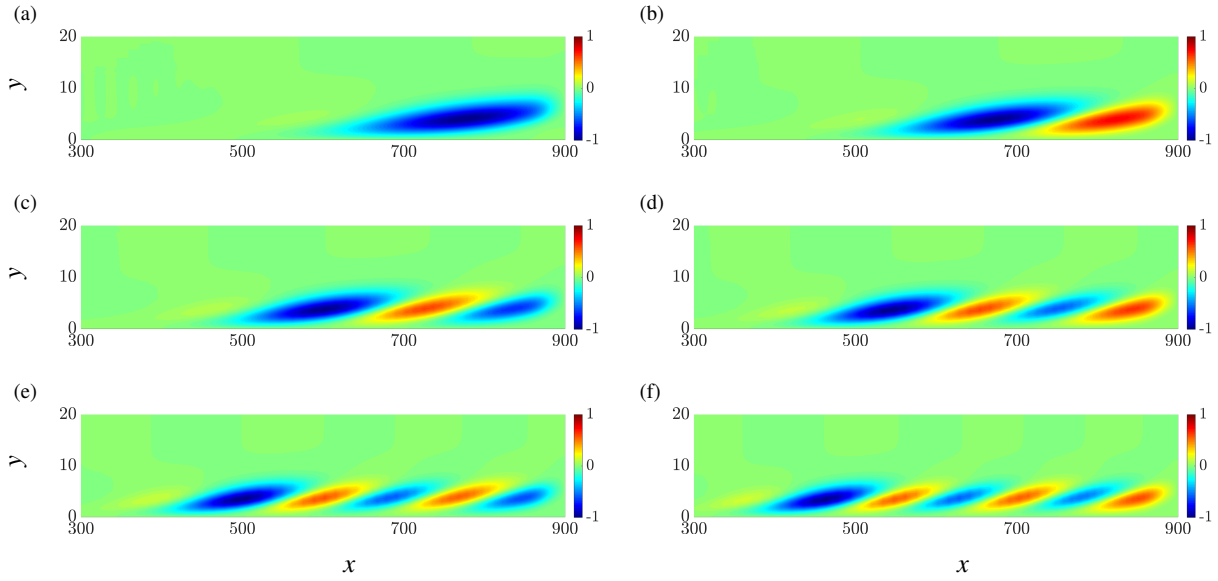

Fig. 12 Streamwise velocity at $z = 0$ corresponding to the first six eigenmodes of the steady-state covariance matrix Φ resulting from near-wall excitation of the boundary layer flow with $Re_0 = 232$ and at $k_z = 0.32$; (a) $j = 1$, (b) $j = 2$, (c) $j = 3$, (d) $j = 4$, (e) $j = 5$, and (f) $j = 6$ where j corresponds to ordering in Fig. 9(a).

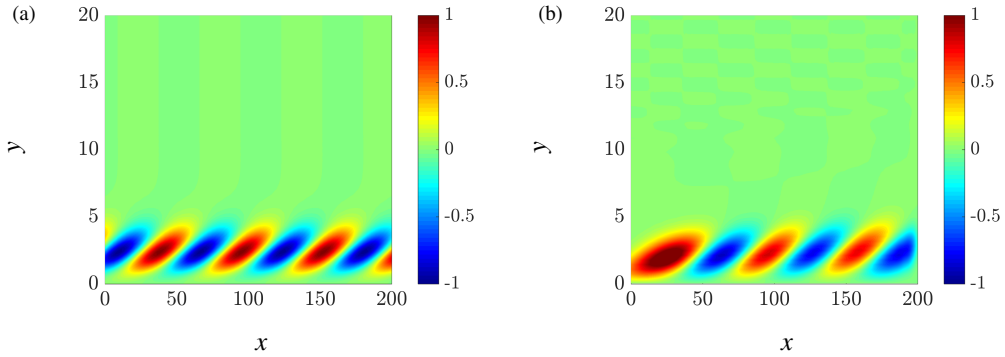

Fig. 13 Streamwise velocity fluctuations resulting from near-wall stochastic excitation of the boundary layer flow. (a) Principal eigenmode of Φ obtained in locally parallel analysis with $Re = 300$ and $(k_x, k_z) = (0.11, 0.32)$; and (b) 6th eigenmode of Φ resulting from global analysis with $k_z = 0.32$. In the global computations $L_x = 200$ and the dominant flow structures appear at $Re \approx 300$.

respectively contain three and four streaks. These streaks become shorter in the streamwise direction and their energy content reduces; see Figs. 12(c) and 12(d). As the mode number increases, the streamwise extent of these structures further reduces, they appear at an earlier streamwise location, and their peak value moves closer to the leading edge. This breakup into shorter streaks for higher modes can be related to the dominant modes identified in locally parallel analysis for increasingly larger streamwise wavenumbers and at various streamwise locations (or Reynolds numbers).

Relations between locally parallel and global analyses

The eigenmodes resulting from locally parallel and global stability analysis are closely related [35, 53]. As shown in the previous sections, both locally parallel and global receptivity analyses predict largest amplification of streamwise elongated structures and the appearance of TS waves. However, the size of flow structures and their wall-normal extent can vary with the streamwise location (Reynolds number). For a proper comparison between the streamwise/wall-normal extent of flow structures, herein, we adjust the Reynolds number used in locally parallel analysis to capture the dominant flow structures toward the end of the global streamwise domain. Moreover, a shorter global domain length L_x should be considered to accommodate subcritical Reynolds numbers ($Re \lesssim 360$) beyond which the local dynamics are unstable. To ensure stability of the global dynamics, we extend the streamwise domain in the upstream direction to $Re_0 = 133$, but for consistency, display results for $Re \geq 232$ after appropriate scaling based on the Blasius length-scale at $Re = 232$.

For near-wall stochastic excitation (case 1 in Table 1), both locally parallel and global receptivity analyses predict the dominant amplification of streamwise elongated structures with $k_z \approx 0.3$; see Figs. 4 and 8. For near-wall excitations with $k_z = 0.32$, Fig. 13 shows that locally parallel analysis of the flow with $Re = 300$ subject to near-wall excitation yieds similar flow structures (with $k_x = 0.11$) to those appearing at $Re \approx 300$ in the 6th eigenmode of the covariance matrix Φ resulting from global analysis. Here, $k_x = 0.11$ is the wavenumber extracted from spatial Fourier transform of the 6th eigenmode of Φ. Moreover, for long spanwise wavelengths, both models predict the amplification of similar TS wave-like structures in the presence of near-wall excitation (see Fig. 14).

We note that in certain scenarios, locally parallel analysis can extract information about streamwise scales that may be hidden in global analysis. This feature can be attributed to the parameterization of the velocity field over streamwise wavenumbers, which enables the separate study of various streamwise length-scales. For example, for wavenumbers at which the global receptivity analysis of the flow subject to outer-layer excitation is dominated by near-wall streaks, locally parallel analysis can uncover the trace of weakly growing outer-layer oscillations at TS frequencies, which is in agreement with the experimental observation of observe outer-layer oscillations; see [48] for additional details.

V. Concluding remarks

We have utilized the algebraic Lyapunov equation to study the receptivity of the Blasius boundary layer flow to white-in-time stochastic forcing entering at various wall-normal locations. Both parallel and global flow analyses predict largest amplification of streamwise elongated streaks with similar spanwise wavelength. Moreover, TS wave-like flow structures arise from persistent near-wall stochastic excitation at long spanwise wavelengths. We have shown that as the

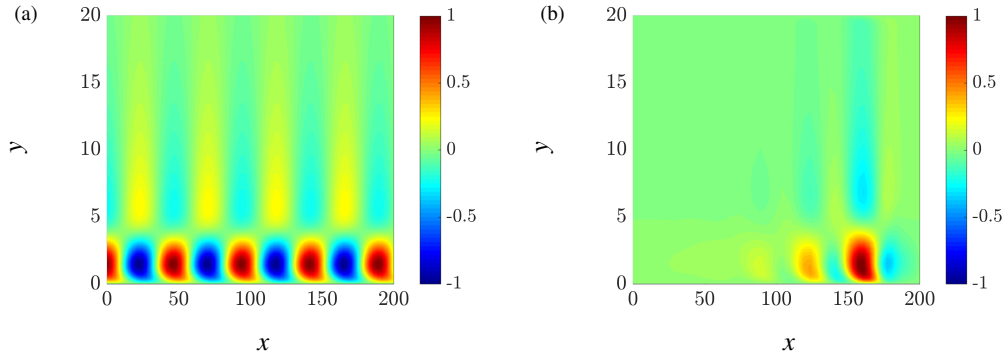

Fig. 14 The TS wave-like spatial structure of the streamwise velocity component of the principal eigenmode of the matrix Φ resulting from near-wall stochastic excitation of the boundary layer flow. (a) Locally parallel analysis with $Re = 300$ and $(k_x, k_z) = (0.13, 0.01)$; and (b) global flow analysis with $k_z = 0.01$. The wavenumber pair for the locally parallel analysis corresponds to the TS wave branch in the energy spectrum of velocity fluctuations. In the global computations $L_x = 200$ and the dominant flow structures appear at $Re \approx 300$.

region of excitation moves away from the wall, energy amplification reduces, which suggests that the near wall region is more sensitive to external disturbances. We have also examined the spatial structure of characteristic eddies that result from stochastic excitation of the boundary layer flow. Our computational experiments demonstrate good agreement between the results obtained from parallel and global flow models and identify the importance of suboptimal flow structures in global analysis. This agreement highlights the efficacy of using parallel flow assumptions in the receptivity analysis of boundary layer flows.

Our Lyapunov-based framework generalizes the concept of receptivity to the amplification of velocity fluctuations from any external source of persistent excitation with known statistical properties. We note that the ability of the method to capture relevant flow physics relies on the spectral properties of the stochastic forcing that can be used to model the effect of, e.g., free-stream turbulence. The spatio-temporal spectrum of stochastic excitation sources can be further determined to correspond to the spectrum of homogeneous isotropic turbulence [48] or to provide statistical consistency with the results of numerical simulations or experimental measurements of the boundary layer flow [25, 59, 60]. Implementation of such ideas to improve physics-based analysis is a topic for future research.

References

[1] Landahl, M. T., "Wave breakdown and turbulence," *SIAM J. Appl. Math.*, Vol. 28, 1975, pp. 735–756.

[2] Landahl, M. T., "A note on an algebraic instability of inviscid parallel shear flows," *J. Fluid Mech.*, Vol. 98, 1980, pp. 243–251.

[3] Orr, W. M. F., "The Stability or Instability of the Steady Motions of a Perfect Liquid and of a Viscous Liquid. Part I: A Perfect Liquid. Part II: A Viscous Liquid." *Proc. R. Irish Acad.*, Vol. 27, 1907, pp. 9–138.

[4] Butler, K. M., and Farrell, B. F., "Three-Dimensional Optimal Perturbations in Viscous Shear Flow," *Phys. Fluids A*, Vol. 4, 1992, p. 1637.

[5] Hack, M. J. P., and Moin, P., "Algebraic disturbance growth by interaction of Orr and lift-up mechanisms," *J. Fluid Mech.*, Vol. 829, 2017, pp. 112–126.

[6] Matsubara, M., and Alfredsson, P. H., "Disturbance Growth in Boundary Layers Subjected to Free-Stream Turbulence," *J. Fluid Mech.*, Vol. 430, 2001, pp. 149–168.

[7] Fransson, J. H. M., Matsubara, M., and Alfredsson, P. H., "Transition induced by free-stream turbulence," *J. Fluid Mech.*, Vol. 527, 2005, pp. 1–25.

[8] Ricco, P., Walsh, E. J., Brighenti, F., and McEligot, D. M., "Growth of boundary-layer streaks due to free-stream turbulence," *Int. J. Heat and Fluid Flow*, Vol. 61, 2016, pp. 272–283.

[9] Jacobs, R., and Durbin, P., "Simulations of bypass transition," *J. Fluid Mech.*, Vol. 428, 2001, pp. 185–212.

[10] Brandt, L., Schlatter, P., and Henningson, D. S., "Transition in boundary layers subject to free-stream turbulence," *J. Fluid Mech.*, Vol. 517, 2004, pp. 167–198.

[11] Goldstein, M. E., "Effect of free-stream turbulence on boundary layer transition," *Phil. Trans. R. Soc. A*, Vol. 372, No. 2020, 2014, p. 20130354.

[12] Hack, M. J. P., and Zaki, T. A., "Streak instabilities in boundary layers beneath free-stream turbulence," *J. Fluid Mech.*, Vol. 741, 2014, pp. 280–315.

[13] Jacobs, R. G., and Durbin, P. A., "Shear sheltering and the continuous spectrum of the Orr-Sommerfeld equation," *Phys. Fluids*, Vol. 10, No. 8, 1998, pp. 2006–2011.

[14] McComb, W. D., *The Physics of Fluid Turbulence*, Oxford University Press, 1991.

[15] Durbin, P. A., and Reif, B. A. P., *Statistical theory and modeling for turbulent flows*, Wiley, 2011.

[16] Orszag, S. A., "Analytical theories of turbulence," *J. Fluid Mech.*, Vol. 41, No. 02, 1970, pp. 363–386.

[17] Kraichnan, R. H., "An almost-Markovian Galilean-invariant turbulence model," *J. Fluid Mech.*, Vol. 47, No. 03, 1971, pp. 513–524.

[18] Monin, A. S., and Yaglom, A. M., *Statistical Fluid Mechanics*, Vol. 2, MIT Press, 1975.

[19] Farrell, B. F., and Ioannou, P. J., "Stochastic Forcing of the Linearized Navier-Stokes Equations," *Phys. Fluids A*, Vol. 5, No. 11, 1993, pp. 2600–2609.

[20] Bamieh, B., and Dahleh, M., "Energy Amplification in Channel Flows with Stochastic Excitation," *Phys. Fluids*, Vol. 13, No. 11, 2001, pp. 3258–3269.

[21] Jovanović, M. R., and Bamieh, B., "Componentwise energy amplification in channel flows," *J. Fluid Mech.*, Vol. 534, 2005, pp. 145–183.

[22] Hwang, Y., and Cossu, C., "Amplification of coherent streaks in the turbulent Couette flow: an input-output analysis at low Reynolds number," *J. Fluid Mech.*, Vol. 643, 2010, pp. 333–348.

[23] Hwang, Y., and Cossu, C., "Linear non-normal energy amplification of harmonic and stochastic forcing in the turbulent channel flow," *J. Fluid Mech.*, Vol. 664, 2010, pp. 51–73.

[24] Moarref, R., and Jovanović, M. R., "Model-based design of transverse wall oscillations for turbulent drag reduction," *J. Fluid Mech.*, Vol. 707, 2012, pp. 205–240.

[25] Zare, A., Jovanović, M. R., and Georgiou, T. T., "Colour of turbulence," *J. Fluid Mech.*, Vol. 812, 2017, pp. 636–680.

[26] Schmid, P. J., and Henningson, D. S., *Stability and Transition in Shear Flows*, Springer-Verlag, New York, 2001.

[27] Herbert, T., "Secondary Instability of Boundary Layers," *Ann. Rev. Fluid Mech.*, Vol. 20, 1988, pp. 487–526.

[28] Leib, S. J., Wundrow, D. W., and Goldstein, M. E., "Effect of free-stream turbulence and other vortical disturbances on a laminar boundary layer," *J. Fluid Mech.*, Vol. 380, 1999, pp. 169–203.

[29] Ricco, P., Luo, J., and Wu, X., "Evolution and instability of unsteady nonlinear streaks generated by free-stream vortical disturbances," *J. Fluid Mech.*, Vol. 677, 2011, pp. 1–38.

[30] Herbert, T., "Parabolized stability equations," *Annu. Rev. Fluid Mech.*, Vol. 29, No. 1, 1997, pp. 245–283.

[31] Lozano-Durán, A., Hack, M. J. P., and Moin, P., "Modeling boundary-layer transition in direct and large-eddy simulations using parabolized stability equations," *Phys. Rev. Fluids*, Vol. 3, No. 2, 2018, p. 023901.

[32] Towne, A., and Colonius, T., "One-way spatial integration of hyperbolic equations," *J. Comput. Phys.*, Vol. 300, 2015, pp. 844–861.

[33] Ran, W., Zare, A., Hack, M. J. P., and Jovanovic, M. R., "Modeling mode interactions in boundary layer flows via Parabolized Floquet Equations," *Phys. Rev. Fluids*, Vol. 4, No. 2, 2019, p. 023901 (22 pages).

[34] Ehrenstein, U., and Gallaire, F., "On two-dimensional temporal modes in spatially evolving open flows: the flat-plate boundary layer," *J. Fluid Mech.*, Vol. 536, 2005, pp. 209–218.

[35] Alizard, F., and Robinet, J., "Spatially convective global modes in a boundary layer," *Phys. Fluids*, Vol. 19, No. 11, 2007, p. 114105.

[36] Nichols, J. W., and Lele, S. K., "Global modes and transient response of a cold supersonic jet," *J. Fluid Mech.*, Vol. 669, 2011, pp. 225–241.

[37] Paredes, P., Gosse, R., Theofilis, V., and Kimmel, R., "Linear modal instabilities of hypersonic flow over an elliptic cone," *J. Fluid Mech.*, Vol. 804, 2016, pp. 442–466.

[38] Schmidt, O. T., Towne, A., Colonius, T., Cavalieri, A. V., Jordan, P., and Brès, G. A., "Wavepackets and trapped acoustic modes in a turbulent jet: coherent structure eduction and global stability," *J. Fluid Mech.*, Vol. 825, 2017, pp. 1153–1181.

[39] Barkley, D., Blackburn, H. M., and Sherwin, S. J., "Direct optimal growth analysis for timesteppers," *Int. J. Numer. Methods Fluids*, Vol. 57, No. 9, 2008, pp. 1435–1458.

[40] Monokrousos, A., Åkervik, E., Brandt, L., and Henningson, D. S., "Global three-dimensional optimal disturbances in the Blasius boundary-layer flow using time-steppers," *J. Fluid Mech.*, Vol. 650, 2010, pp. 181–214.

[41] Brandt, L., Sipp, D., Pralits, J. O., and Marquet, O., "Effect of base-flow variation in noise amplifiers: the flat-plate boundary layer," *J. Fluid Mech.*, Vol. 687, 2011, pp. 503–528.

[42] Jeun, J., Nichols, J. W., and Jovanović, M. R., "Input-output analysis of high-speed axisymmetric isothermal jet noise," *Phys. Fluids*, Vol. 28, No. 4, 2016, p. 047101 (20 pages).

[43] Schmidt, O. T., Towne, A., Rigas, G., Colonius, T., and Brès, G. A., "Spectral analysis of jet turbulence," *J. Fluid Mech.*, Vol. 855, 2018, pp. 953–982.

[44] Dwivedi, A., Sidharth, G. S., Nichols, J. W., Candler, G. V., and Jovanovic, M. R., "Reattachment vortices in hypersonic compression ramp flow: an input-output analysis," *J. Fluid Mech.*, Vol. 880, 2019, pp. 113–135.

[45] Trefethen, L. N., Trefethen, A. E., Reddy, S. C., and Driscoll, T. A., "Hydrodynamic Stability Without Eigenvalues," *Science*, Vol. 261, 1993, pp. 578–584.

[46] Jovanović, M. R., "Modeling, analysis, and control of spatially distributed systems," Ph.D. thesis, University of California, Santa Barbara, 2004.

[47] McKeon, B. J., and Sharma, A. S., "A critical-layer framework for turbulent pipe flow," *J. Fluid Mech.*, Vol. 658, 2010, pp. 336–382.

[48] Ran, W., Zare, A., Hack, M. J. P., and Jovanovic, M. R., "Stochastic receptivity analysis of boundary layer flow," *Phys. Rev. Fluids*, Vol. 4, No. 9, 2019, p. 093901 (28 pages).

[49] Weideman, J. A. C., and Reddy, S. C., "A MATLAB Differentiation Matrix Suite," *ACM Trans. Math. Software*, Vol. 26, No. 4, 2000, pp. 465–519.

[50] Kwakernaak, H., and Sivan, R., *Linear optimal control systems*, Wiley-Interscience, 1972.

[51] Bakewell, H. P., and Lumley, J. L., "Viscous sublayer and adjacent wall region in turbulent pipe flow," *Phys. Fluids*, Vol. 10, No. 9, 1967, pp. 1880–1889.

[52] Moin, P., and Moser, R., "Characteristic-eddy decomposition of turbulence in a channel," *J. Fluid Mech.*, Vol. 200, No. 41, 1989, p. 509.

[53] Huerre, P., and Monkewitz, P. A., "Local and global instabilities in spatially developing flows," *Annu. Rev. Fluid Mech.*, Vol. 22, No. 1, 1990, pp. 473–537.

[54] Andersson, P., Berggren, M., and Henningson, D., "Optimal disturbances and bypass transition in boundary layers," *Phys. Fluids*, Vol. 11, No. 1, 1999, pp. 134–150.

[55] Luchini, P., "Reynolds-number-independent instability of the boundary layer over a flat surface: optimal perturbations," *J. Fluid Mech.*, Vol. 404, 2000, pp. 289–309.

[56] Hack, M. J. P., and Zaki, T. A., "Modal and non-modal stability of boundary layers forced by spanwise wall oscillations," *J. Fluids Mech.*, Vol. 778, 2015, pp. 389–427.

[57] Theofilis, V., "Advances in global linear instability analysis of nonparallel and three-dimensional flows," *Prog. Aerosp. Sci.*, Vol. 39, No. 4, 2003, pp. 249–315.

[58] Ran, W., Zare, A., Nichols, J. W., and Jovanović, M. R., "The effect of sponge layers on global stability analysis of Blasius boundary layer flow," *Proceedings of the 47th AIAA Fluid Dynamics Conference*, Denver, CO, 2017, p. 3456 (12 pages).

[59] Zare, A., Chen, Y., Jovanović, M. R., and Georgiou, T. T., "Low-complexity modeling of partially available second-order statistics: theory and an efficient matrix completion algorithm," *IEEE Trans. Automat. Control*, Vol. 62, No. 3, 2017, pp. 1368–1383.

[60] Zare, A., Georgiou, T. T., and Jovanovic, M. R., "Stochastic dynamical modeling of turbulent flows," *Annu. Rev. Control Robot. Auton. Syst.*, Vol. 3, 2020. In press; doi:10.1146/annurev-control-053018-023843; also arXiv:1908.09487.